2024 IEEE 63rd Conference on Decision and Control (CDC)
December 16-19, 2024. MiCo, Milan, Italy

Closed-Loop Peripheral Nerve Stimulation for the Restoration of Normal Pain Processing

Patrick Myers, Yun Hwang, Daniel Ehrens, Christine Beauchene, Xiang Cui, Sergey Khasabov, Yun Guan, Sridevi Sarma

Abstract— Neuropathic chronic pain, caused by nerve injury, is common and debilitating. Pharmaceuticals, the primary treatment, often lead to severe side effects. Electrical stimulation is a promising alternative with fewer side effects, but its efficacy is limited. Most clinical neuromodulation methods are open-loop, with settings adjusted during office visits, leading to reduced effectiveness over time. Proposed closed-loop strategies typically activate when a pain signal crosses a threshold, acting like an anesthetic by removing all pain. However, since acute pain has a protective role, the ideal therapy should target chronic pain while preserving acute pain responses. We present a proof-of-concept for a model-based closed-loop neuromodulation therapy aimed at normalizing pain responses in neuropathic rats. By measuring evoked pain responses from thalamic local field potentials in nerve-injured and naïve rats, we estimate transfer functions for both groups. We then use a model matching approach to quantify the difference between the nerve-injured and ideal (naïve) system responses as the error signal. Finally, we design an optimal controller using H-infinity methods to minimize this error and control input within relevant frequency bands. **The resulting in-silico experiment provides a foundation for a more biologically realistic controller design which can be implemented in-vivo.**

I. Introduction

Pain is a universal experience. Acute pain is an early-warning physiological signal triggered in the nervous system, essential to detect and minimize contact with damaging or noxious stimuli. However, the nervous system responsible for the protective, nociceptive pain processing is fragile as inflammation, damage, and malfunction of the nervous system may divert its function, creating a debilitating disease known as neuropathic chronic pain (NCP). NCP is defined as pain that lasts beyond the time it takes to heal a wound or longer than 12 weeks and affects about 100 million American adults—more than the total affected by heart disease, cancer, and diabetes combined. It costs the nation $560–635 billion each year in medical expenses and lost productivity [1]. Chronic pain is primarily treated with neuropharmacology, which may be inadequate or toxic, have negative side effects, and lose efficacy after long term use [2]. In fact, chronic pain has been linked to opioid dependence, as well as the resultant opioid epidemic [3]. Further, pain contributes to anxiety and depression, as well as reduced quality of life [1].

A highly promising alternative to drug treatment with fewer side effects is neuromodulation via electrical stimulation of nerve fibers [4], [5]]. However, these therapies have been associated with suboptimal efficacy and limited long-term success as they are currently (i) trial-and-error therapeutic approaches, (ii) they primarily operate in open-loop, i.e., the stimulation parameters do not automatically adjust to fluctuations of the diseased state of the pain system, and (iii) their mechanisms of action remain unclear [6]. A few closed-loop (CL) approaches that adapt the spinal cord stimulation parameters to pain signals have been proposed to treat chronic pain [7], [8], but they simply turn on suppressive stimulation when specific pain signals exceed a threshold. The goal of current CL systems is to *suppress all pain*, including acute pain that alerts the body to damaging stimuli. We need a systematic model-driven approach to optimize (based on model predictions and not trial and error) adaptive neurostimulation treatment that aims to restore the pain system back to health, i.e., suppressing pathological pain while transmitting acute pain.

In this paper, we describe our approach to designing a model-based closed loop neuromodulation therapy (CLNT) that restores the nervous system response of a nerve injured

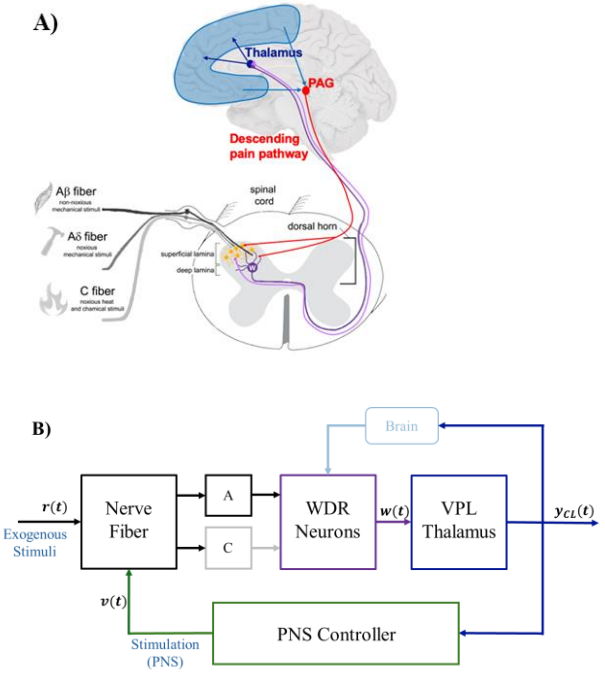

Figure 1. A. The pain system, including ascending and descending pain pathways. Pain and touch information from the periphery converge on WDR (W) neurons in the spinal cord. These signals are transmitted to the brain for further processing. **B.** Block diagram of pain system and our proposed closed-loop PNS feedback controller.

animal to that of a healthy animal based on an electrophysiological recording of neural activity in the rat's brain, which in turn informs PNS treatment. See **Fig. 1** for schematic of biological pain system (**Fig. 1A**) and our closed-loop system (**Fig. 1B**).

II. Methods

A. Electrophysiological Recordings

Adult male Sprague-Dawley rats (300-400g) were used for this experiment. All procedures were approved by the Johns Hopkins Animal Care and Use Committee. A tibial spared nerve injury (SNI-t) model, sparing the tibial branch of the sciatic nerve, was used to simulate neuropathic chronic pain, as described here [9]. Before performing the SNI procedure, the rat's pain threshold was assessed via a paw withdrawal test (PWT). In this test, calibrated Von Frey filaments are applied to the hind paw of the rat in the receptive field of the tibial nerve. The weight of the filament is increased until the rat withdraws its paw. Using this starting weight, a simplified up-down (SUDO) procedure was performed to determine the baseline PWT of the rat [10]. The rat was then anesthetized with 1.5% isoflurane and the SNI-t procedure was performed, and the surgical site was closed. After 7-14 days, the animal is expected to have peak neuropathic pain [9]. The SUDO procedure is repeated to find the new PWT of the rat to confirm the expected decrease caused by the neuropathic pain induction.

Neural activity was then recorded from both the nerve injured and naïve rats. The rats were induced with isoflurane and then paralyzed via intraperitoneal injection of urethane (10% concentration at 1% of body weight). The prepared rats were then head-fixed into a stereotaxic frame on a noise isolation table, and the yaw, pitch, and roll of the frame were adjusted so the skull was square to the referential axis. A 1.5mm square craniotomy on the contralateral (right) side to the sciatic nerve of interest was performed. A single tungsten microelectrode (World Precision Instruments) was then inserted into the ventral posterolateral (VPL) nucleus of the thalamus in the brain, an important sensory relay point in the ascending pain pathway [11]. The recording location of 3.4mm ML, -3mm AP, 6mm DV relative to the bregma was selected according to the rat brain atlas [12]. The sciatic nerve of the left hind leg was then exposed and placed on a bipolar platinum hook electrode. The microelectrode location in the brain was then adjusted by analyzing the strength of the stimulation response evoked by a pulse stimulation at the sciatic nerve.

Evoked LFPs were then recorded. A single pulse stimulus train was applied to the exposed sciatic nerve at 1mA. Fifteen pulses of 0.25ms width were applied at 0.1Hz. Next, an open-loop stimulation mimicking clinical PNS (50Hz for 5 minutes) was applied to the sciatic nerve. After the treatment, the evoked LFP protocol was repeated to measure the effect of the therapeutic stimulation. Data was recorded using Tucker-Davis technologies (TDT) Synapse software.

B. Data Preprocessing

A notch filter at the powerline frequency, 60Hz, and its harmonics was applied to the data. A band-pass filter from 0.5 to 300Hz was then applied. Recordings were split into individual trials based on the pulses applied to the sciatic nerve. Trials were shifted so that the neural activity before the stimulus was averaged to 0mV to remove any electrode drift. Since the stimulus was applied at 0.1Hz, we do not expect any accumulating windup effect to be present in subsequent trials.

C. Defining the Evoked Response in the Brain

Since recording evoked potentials in the VPL from a PNS input is a unique experiment, we first needed to define the expected response shape for this activity. For each trial, 0.1 seconds before and 1.2 seconds after the stimulus were analyzed. Points of interest, namely the positive and negative peaks, are denoted in **Fig. 2**. We then estimate which nerve fiber types are contributing to these points based on the conduction velocities of the various fibers (**see Discussion section for further analysis**). We expect the early portion of the response to be solely caused by fast activity from the myelinated Aα/ß fibers, while the later components are caused by a combination of the fast fibers and the unmyelinated C fibers.

Peripheral nerves contain multiple fiber types which encode different stimuli (**Fig. 1A**). Aα and Aß fibers are large, heavily myelinated fibers with fast conduction velocities that encode non-noxious stimuli such as touch. Aδ fibers are smaller, also heavily myelinated, and have a slightly slower conduction velocity, encoding for fast noxious stimuli. C fibers are small, unmyelinated, and have a slow conduction velocity. C fibers encode for slow noxious stimuli. Information that is being transmitted via a peripheral nerve, such as the single pulse stimulation on the sciatic nerve, is carried at different rates based on which fibers are performing the transmission. In prior studies, it has been shown that C fiber-based activity within WDR neurons of the spinal cord is

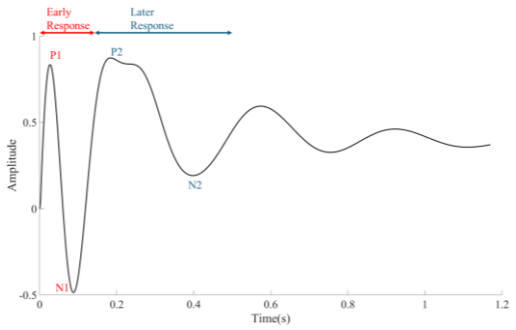

Figure 2: Characterization of the evoked response in the VPL in the brain. The early response, which is likely related to non-noxious encoding, contains two sharp peaks: P1, and N1. The later portion of the response, which contains two slower peaks (P2 and N2), potentially corresponds to C-fiber mediated activity and is of interest as these fibers encode noxious stimuli.

a good biomarker of chronic pain [13]. Our initial attempt to define the evoked response in the VPL uses a similar approach of delineating based on the latency of the components. Since

our recording location is multiple synapses away from the stimulus and has receives multiple inputs not directly related to the pathway of interest, we expect the characterization of the response to be more complicated than that in the spinal cord.

D. Predicting System Response Using LTI Models

The pain processing pathway is likely a nonlinear process, as the transference of information up ascending pathways (towards the brain) is modulated by a descending pathway (towards the peripheral nervous system), as described in the Gate Control Theory of pain processing [14]. Several attempts have been made to construct biophysical models of this nerve fiber activation [15], [16]. While these models do provide some insight into the neurophysiology of pain, they are all high dimensional and non-linear, and are therefore not great candidates for tractable, real time closed-loop control applications.

Instead, we aim to assess whether a linear time-invariant model can be used to characterize VPL activity and to develop a closed-loop neuromodulation therapy. The first step is to determine how the input (the single pulse PNS on the sciatic nerve) is modulated along its path up the spinothalamic tract (STT) to the observed output (the LFP activity in the VPL). See Fig. 3. Using a linear time-invariant (LTI) model, we characterized the system with the equation:

$$Y(s) = G(s)R(s), \tag{1}$$

where s is the Laplace variable, $R(s)$ is the single pulse stimulus reference input, $G(s)$ is the plant representing the pathway of the STT that the signal travels through, and $Y(s)$ is our recorded output at the VPL. The STT model has the form:

$$G(s) = \frac{b_z s^z + b_{z-1} s^{z-1} + b_{z-2} s^{z-2} + \cdots + b_0}{s^p + a_{p-1} s^{p-1} + a_{p-2} s^{p-2} + \cdots + a_0}, \tag{2}$$

where $\vec{a}$ and $\vec{b}$ are coefficients fitted using MATLAB's *tfest* function as described here [29], and p and z are the number of poles and zeros, respectively. We omit the time delay term for simplicity as we assume no time delay in our estimation. One major challenge of fitting transfer functions to neurophysiological data is the recorded LFP signal captures activity directly related to the evoked response and unrelated neural activity in close proximity to the recording electrode. To limit the impact of this unrelated activity, we used the average of the evoked trials as $Y(s)$. Limiting the model complexity to prevent fitting high frequency oscillations also helps reduce the impact of the background neural signals.

The number of poles and zeros was determined via a grid search, allowing the poles and zeros to range from 4 to 8. The upper bound on model complexity was set to prevent overfitting. For each potential transfer function estimation, the corresponding evoked response was simulated by inputting an impulse into the model. This estimated response was compared to the actual average response and the transfer function that produced the smallest root means squared error between the real-averaged and estimated responses was chosen.

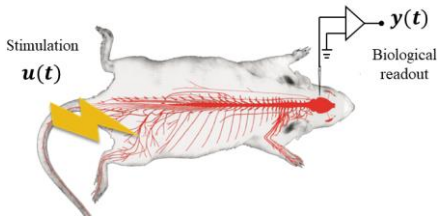

Figure 3: Experimental design. Local field potentials are read from the VPL in the brain. This readout is the input to a controller, *K*, which outputs a signal to use for peripheral nerve stimulation of the sciatic nerve.

E. Model-Matching Control

The control objective for this work is to approximate the neural activity of the healthy rat by adding a controller that modulates the neural activity of the neuropathic rat. To accomplish this goal, we use a model-matching scheme as shown in **Fig. 4**. The model representing the naïve rat, G_N, is the ideal system, and the plant representing the injured rat, G_I, is controlled by the controller, K. An error term, $e(t)$, representing the difference in output of the two systems, $y_N(t)$ and $y_I(t)$ respectively, to the exogenous impulse input, $r(t)$, was constructed. This error term is provided as input to the controller, which produces a control input, $u(t)$. The control input is added to r(t) to create a closed-loop input for G_I.

To identify an optimal K, we constructed two performance functions: z_e and z_u, in the form of:

$$z_e = W_e E(s), \tag{3}$$

$$z_u = W_u U(s), \tag{4}$$

where W_e and W_u are frequency-specific weighting functions. Specifically, the weighting functions were designed to limit the error between the naïve and closed-loop injured responses within biologically relevant low frequencies and the control input within high frequencies. We

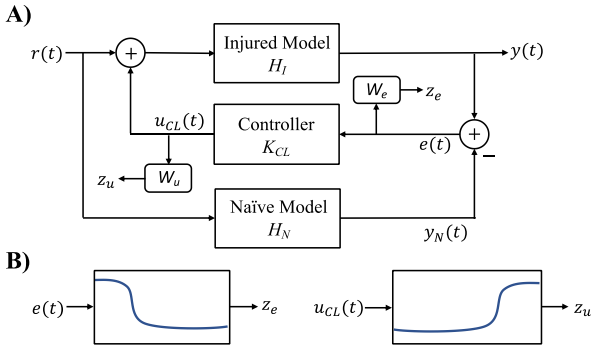

Figure 4: Design of the controller to normalize the pain response in a neuropathic rat. A) Block diagram of the model-matching scheme which attempts to control the VPL activity of an injured rat, y(t), to that of a healthy rat, $y_H(t)$. B) Weighting functions used to generate performance metrics on the error, e(t), and control input, u(t), for H_∞ synthesis.

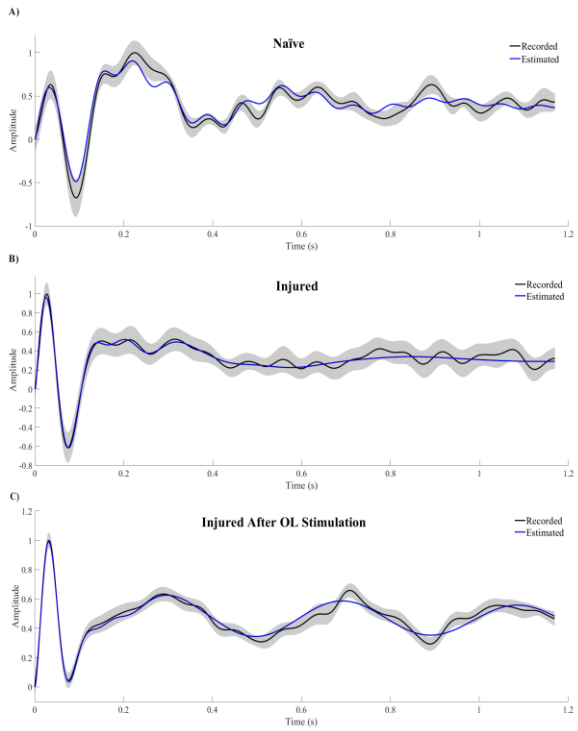

Figure 5: Model estimation of evoked responses for (A) a naïve rat, (B) a neuropathic rat, and (C) a neuropathic rat after open loop PNS. The standard error across the 15 recorded trials is represented by the shaded region around the black solid line for each respective experiment.

then searched for a K that solved the following minimization equation:

$$\underset{K \text{ stabilizing}}{min} \left\| \begin{matrix} z_e \\ z_u \end{matrix} \right\|_\infty, \tag{5}$$

using H_∞ synthesis methods in MATLAB [30], [31], [32], [33], [34].

II. Results

A. Evoked Responses Shape Changes After Nerve Injury

Fig. 5 shows the evoked VPL activity for the naïve and nerve injured rats. For the first 150ms after the stimulus, the naïve rat appears to have the two strong peaks P1 and N1, as denoted in **Fig. 2**. This portion of the response is likely transmitted by the faster nerve fibers (Aα/ß), which encode non-noxious stimuli. From 150ms to 500ms, the naïve rat's response contains a high amplitude, wide peak (P2) and a small negative amplitude, wide peak (N2). This portion of the response could be transmitted by the slower C-fibers, which encode noxious stimuli. In contrast, the nerve injured rat's initial components seem to occur slightly earlier, with P1 occurring around 25ms and N1 occurring around 75ms. The later components of the neuropathic rat's response are smaller in amplitude, with N2 being barely detectable.

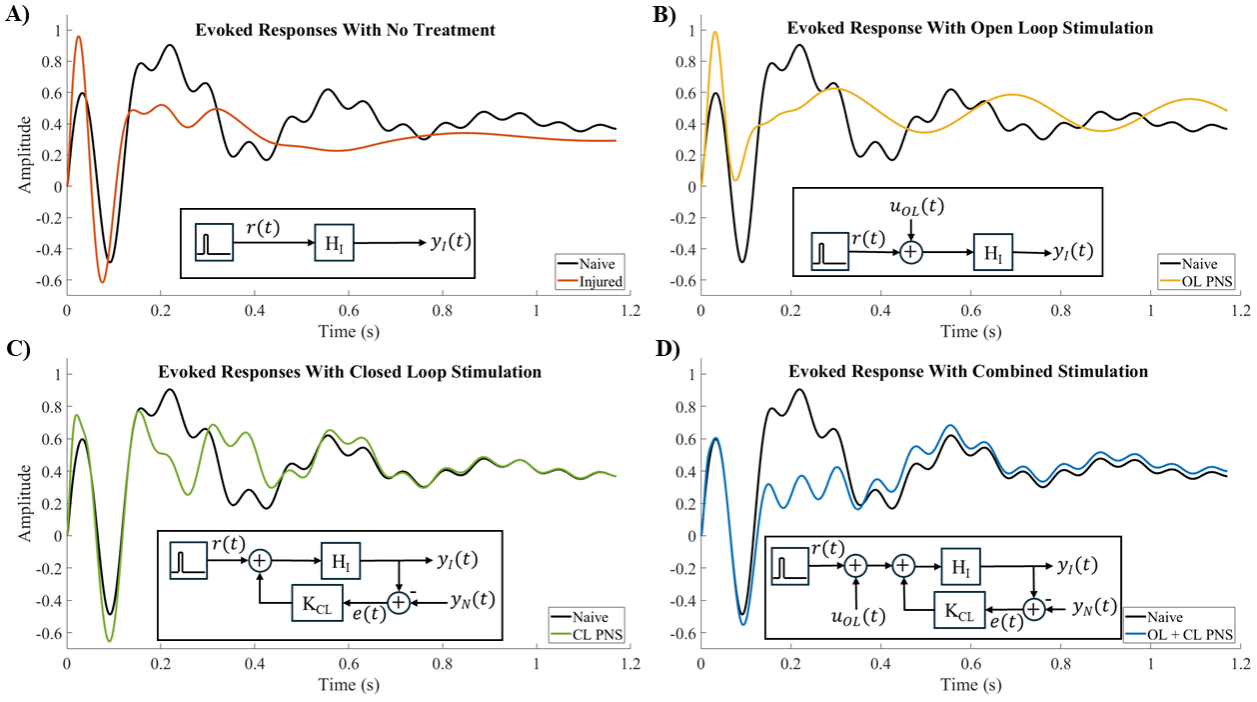

Figure 6: Estimated evoked responses in the VPL in the brain from a single pulse stimulation of the contralateral sciatic nerve. **A)** Naïve (black line), injured (orange line), and **B)** open loop PNS (yellow line) groups are estimated from experimentally recorded responses, while the **C)** closed loop PNS (green line) and **D)** combined PNS (blue line) groups are the estimated response of the closed-loop systems with an exogenous impulse input. The associated block diagram to generate each response is included in the respective plot.

B. Model Estimation Can Recreate VPL Response

Linear time-invariant models were estimated for both the naïve and neuropathic rats. The fit was assessed by comparing the output estimated by the models to an impulse input to the actual recorded response. **Fig. 5** shows the actual average VPL response (black line) and the estimated response (blue line) for **a)** the naïve rat and **b)** the neuropathic rat, and **c)** the same neuropathic rat after receiving the open loop PNS treatment.

C. H_∞ Controller Approximates Healthy Response to Impulse Stimulus

Fig. 6 shows the estimated naïve rat response (black line), **a)** injured rat response (orange line), **b)** and injured rat response after open loop PNS treatment (yellow line) from experimental data, and **c)** the estimated injured rat response in closed-loop (green line) and **d)** estimated injured rat response with a combination of the open loop and closed loop stimulations (blue line). The controller in **c)** was able to steer the injured response towards the naïve response to an impulse stimulus, specifically by better aligning the early components and by reviving the higher frequency activity of the later portion of the response. The controller in **d)** showed marginal improvement over the controller in **c)** by better aligning the early components and N2.

III. Discussion and Future work

Prior work has demonstrated that neuropathic rats have an increased spontaneous firing rate of WDR neurons in the spinal cord [20] and VPL neurons [35]. Within the spinal cord, it has also been shown that the C-component of the evoked response increases after nerve injury [20]. Yet there is no work, to our knowledge, that analyzes the evoked activity of VPL neurons to an electrical stimulation of a peripheral nerve. For our novel experiment, we found that the early components of the evoked response are similar for both naïve and neuropathic rats. The later, potentially C-driven, component of the response varied between the two populations. The change in response after nerve injury initially appears contrary to what was observed in the spinal cord. However, single-cell recordings were performed in the spinal cord whereas local field potentials, which record population activity from hundreds to thousands of neurons, were recorded from the VPL. Two possible explanations for this phenomenon are (1) the increased spontaneous firing rate of these neurons makes it more difficult for them to respond to a stimulus and (2) while individual neurons have an increased firing rate, the simultaneous recruitment of neurons necessary to see large LFP changes is lessened.

With the current experiment design, we are unable to definitively label which nerve fiber types contribute to each component of the evoked response. In future work, we will utilize the peripherally acting opioid dermorphin [D-Arg2, Lys4] (1–4) amide (DALDA), which has been shown to selectively inhibit C-fiber activation [36]. The portions of the response that remain after DALDA injection will be attributed to A-fiber activation, and the removed components will be attributed to C-fiber activation. This knowledge could aid in future control design, allowing for biologically motivated objective functions that focus on normalizing C-fiber activity.

References

[1] R. L. Nahin, "Estimates of pain prevalence and severity in adults: United States, 2012," *J. Pain*, vol. 16, no. 8, pp. 769–780, Aug. 2015, doi: 10.1016/j.jpain.2015.05.002.

[2] R. A. Moore and H. J. McQuay, "Prevalence of opioid adverse events in chronic non-malignant pain: systematic review of randomised trials of oral opioids," *Arthritis Res. Ther.*, vol. 7, no. 5, pp. R1046-1051, 2005, doi: 10.1186/ar1782.

[3] P. Skolnick, "The Opioid Epidemic: Crisis and Solutions," *Annu. Rev. Pharmacol. Toxicol.*, vol. 58, no. Volume 58, 2018, pp. 143–159, Jan. 2018, doi: 10.1146/annurev-pharmtox-010617-052534.

[4] A. Conger *et al.*, "The Effectiveness of Spinal Cord Stimulation for the Treatment of Axial Low Back Pain: A Systematic Review with Narrative Synthesis," *Pain Med. Malden Mass*, vol. 21, no. 11, pp. 2699–2712, Nov. 2020, doi: 10.1093/pm/pnaa142.

[5] "Neuromodulation | For Consumers | Abbott U.S." Accessed: Jan. 03, 2024. [Online]. Available: https://www.abbott.com/consumer/neuromodulation.html

[6] S. Helm *et al.*, "Peripheral Nerve Stimulation for Chronic Pain: A Systematic Review of Effectiveness and Safety," *Pain Ther.*, vol. 10, no. 2, pp. 985–1002, Dec. 2021, doi: 10.1007/s40122-021-00306-4.

[7] A. Farajidavar, C. E. Hagains, Y. B. Peng, and J.-C. Chiao, "A closed loop feedback system for automatic detection and inhibition of mechano-nociceptive neural activity," *IEEE Trans. Neural Syst. Rehabil. Eng. Publ. IEEE Eng. Med. Biol. Soc.*, vol. 20, no. 4, pp. 478–487, Jul. 2012, doi: 10.1109/TNSRE.2012.2197220.

[8] M. Russo *et al.*, "Effective Relief of Pain and Associated Symptoms With Closed-Loop Spinal Cord Stimulation System: Preliminary Results of the Avalon Study," *Neuromodulation J. Int. Neuromodulation Soc.*, vol. 21, no. 1, pp. 38–47, Jan. 2018, doi: 10.1111/ner.12684.

[9] X. Cui *et al.*, "Enhancing spinal cord stimulation-induced pain inhibition by augmenting endogenous adenosine signalling after nerve injury in rats," *Br. J. Anaesth.*, vol. 132, no. 4, pp. 746–757, Apr. 2024, doi: 10.1016/j.bja.2024.01.005.

[10] R. P. Bonin, C. Bories, and Y. De Koninck, "A simplified up-down method (SUDO) for measuring mechanical nociception in rodents using von Frey filaments," *Mol. Pain*, vol. 10, p. 26, Apr. 2014, doi: 10.1186/1744-8069-10-26.

[11] P. R. Kramer *et al.*, "Role for the Ventral Posterior Medial/Posterior Lateral Thalamus and Anterior Cingulate Cortex in Affective/Motivation Pain Induced by Varicella Zoster Virus," *Front. Integr.*

Neurosci., vol. 11, 2017, Accessed: Feb. 10, 2023. [Online]. Available: https://www.frontiersin.org/articles/10.3389/fnint.2017.00027

[12] G. Paxinos and C. Watson, *The Rat Brain in Stereotaxic Coordinates*, 7th ed. Academic Press, 2013.

[13] Y. Guan *et al.*, "Spinal cord stimulation-induced analgesia: electrical stimulation of dorsal column and dorsal roots attenuates dorsal horn neuronal excitability in neuropathic rats," *Anesthesiology*, vol. 113, no. 6, pp. 1392–1405, Dec. 2010, doi: 10.1097/ALN.0b013e3181fcd95c.

[14] R. Melzack and P. D. Wall, "Pain Mechanisms: A New Theory," *Science*, vol. 150, no. 3699, pp. 971–979, Nov. 1965, doi: 10.1126/science.150.3699.971.

[15] C. Solanes, J. L. Durá, M. Ángeles Canós, J. De Andrés, L. Martí-Bonmatí, and J. Saiz, "3D patient-specific spinal cord computational model for SCS management: potential clinical applications," *J. Neural Eng.*, vol. 18, no. 3, Mar. 2021, doi: 10.1088/1741-2552/abe44f.

[16] C. D. Mørch, G. P. Nguyen, P. W. Wacnik, and O. K. Andersen, "Mathematical Model of Nerve Fiber Activation During Low Back Peripheral Nerve Field Stimulation: Analysis of Electrode Implant Depth," *Neuromodulation Technol. Neural Interface*, vol. 17, no. 3, pp. 218–225, Apr. 2014, doi: 10.1111/ner.12163.

[17] A. Arda Ozdemir and S. Gumussoy, "Transfer Function Estimation in System Identification Toolbox via Vector Fitting," *IFAC-Pap.*, vol. 50, no. 1, pp. 6232–6237, Jul. 2017, doi: 10.1016/j.ifacol.2017.08.1026.

[18] K. Glover and J. C. Doyle, "State-space formulae for all stabilizing controllers that satisfy an $H\infty$-norm bound and relations to relations to risk sensitivity," *Syst. Control Lett.*, vol. 11, no. 3, pp. 167–172, Sep. 1988, doi: 10.1016/0167-6911(88)90055-2.

[19] J. Doyle, K. Glover, P. Khargonekar, and B. Francis, "State-space solutions to standard H2 and H∞ control problems," in *1988 American Control Conference*, Jun. 1988, pp. 1691–1696. doi: 10.23919/ACC.1988.4789992.

[20] M. G. SAFONOV, D. J. N. LIMEBEER, and R. Y. CHIANG, "Simplifying the H∞ theory via loop-shifting, matrix-pencil and descriptor concepts," *Int. J. Control*, vol. 50, no. 6, pp. 2467–2488, Dec. 1989, doi: 10.1080/00207178908953510.

[21] P. Gahinet and P. Apkarian, "A linear matrix inequality approach to H∞ control," *Int. J. Robust Nonlinear Control*, vol. 4, no. 4, pp. 421–448, 1994, doi: 10.1002/rnc.4590040403.

[22] T. Iwasaki and R. E. Skelton, "All controllers for the general H<math><mtext>H</mtext></math>∞ control problem: LMI existence conditions and state space formulas," *Automatica*, vol. 30, no. 8, pp. 1307–1317, Aug. 1994, doi: 10.1016/0005-1098(94)90110-4.

[23] V. Tiwari *et al.*, "Activation of Peripheral Mu-Opioid Receptors by Dermorphin [D-Arg2, Lys4] (1-4) amide Leads to Modality-preferred Inhibition of Neuropathic Pain," *Anesthesiology*, vol. 124, no. 3, pp. 706–720, Mar. 2016, doi: 10.1097/ALN.0000000000000993.